

# Energy saving and performance analysis of air-cooled photovoltaic panels

Wisam K. Hussam<sup>1,2</sup>  | Ali M. Khlefat<sup>1</sup> | Gregory J. Sheard<sup>2</sup>

<sup>1</sup>School of Engineering, Australian College of Kuwait, Safat, Kuwait

<sup>2</sup>Department of Mechanical and Aerospace Engineering, Monash University, Melbourne, Victoria, Australia

## Correspondence

Wisam K. Hussam, School of Engineering, Australian College of Kuwait, Safat, Kuwait.

Email: w.alsaadi@ack.edu.kw

## Funding information

Australian Research Council, Grant/Award Number: DP180102647; Kuwait Foundation for the Advancement of Sciences, Grant/Award Number: PN19-35EM-02

## Summary

The efficiency of photovoltaic (PV) cells is known to degrade with temperature, which limits their efficacy in the many regions around the world having a climate featuring high ambient temperatures. This study reports on field experiments supported by numerical modelling using Ansys steady-state thermal solver that demonstrates improved PV cell performance when coupled with a passive natural-convection-driven heat sink. Heat sink fin spacing was optimized for hot climatic conditions. Experiments were conducted on a pair of PV modules, one fitted with the heat sink, the other serving as a control. Temperature data were acquired at 15 minute intervals from 6.00 AM to 5.30 PM at both the front and rear of the modules. The heat sink respectively improved solar-to-electrical conversion efficiency and power output by 35% and almost 55%, and led to panel temperature reductions of up to 4°C and 3°C.

## KEYWORDS

3D simulation, efficiency improvement, natural convection, optimized heat sink, photovoltaic cell

## 1 | INTRODUCTION

Electricity generation in Kuwait is reliant on primary energy sources such as oil and natural gas, which is contributing to the depletion of non-renewable resources and environmental damage. Electricity consumption in Kuwait has increased more than one hundredfold over the last five decades, from 380 GWh in 1960 to 45 TWh in 2008. This has been driven by both a rise in population and per capita electricity consumption. Over 2000 to 2009, the population growth of 3.9% per annum was surpassed by the 6.8% per annum growth in per capita electricity usage.<sup>1</sup> Therefore, there is an essential need to diversify away from these sources and pursue alternatives such as solar and wind energy.

Due to the abundance of sunlight throughout the year in this region, solar energy is an ideal candidate for renewable power generation over wind energy. Kuwait experiences an attractive rate of solar radiation ranging

over 3.5 to 8.0 kWh/m<sup>2</sup>/day.<sup>2</sup> The highest average hourly radiation is attained in Summer during the months of May to September at 12.00 PM, peaking in June, while the lowest average occurs in the Winter months, with January recording the minimum average value.<sup>3</sup> The daily average temperature in the winter season is 14.4°C while it often exceeds 48°C in the summer season.

Photovoltaic (PV) solar cells directly convert sunlight into electrical energy via the photovoltaic effect: when solar radiation passes through a PV panel, part of the energy is converted into electrical energy, while the rest is converted into heat. This heat is dissipated to the surroundings by convection and radiation from the front and rear surfaces of the panel. In contemporary PV cells, solar radiation is converted over a small band of wavelengths from 0.4 to 1.1 nanometre, limiting the maximum efficiency for conversion of solar radiation to electricity of less than 20%.<sup>4,5</sup>

Temperature is key to the efficiency of PV cells, as power output decreases with increasing temperature of

the PV substrate.<sup>6-11</sup> The power output decrease experienced by a PV module is approximately  $0.5\%/^{\circ}\text{C}$ .<sup>12</sup> Previous studies<sup>13,14</sup> revealed that the temperature effect on the efficiency of a PV module is more significant for c-Si modules than for other types (eg, amorphous silicon solar cells<sup>15,16</sup> and thin-film cadmium telluride cells<sup>17,18</sup>). At solar irradiance levels above  $\approx 950\text{ W/m}^2$ , cell temperatures exceed  $60^{\circ}\text{C}$ , and efficiency falls to approximately 9%.<sup>11</sup>

The lifespan and efficiency of a PV cell can be enhanced, particularly in locations having a hot climate, using strategies such as active or passive cooling systems.<sup>19,20</sup> Passive cooling is an effective, cheap and practical cooling approach that eliminates the complexity, expense and reliability considerations of powered components such as fans, etc. A passive cooling approach that has been explored involves the use of a plate-fin heat sink, where the extended surface area of thermally conducting fins is used to cool PV cells via natural convection (ie, flow driven by buoyancy differences between hot and cold air). Comprehensive reviews of experimental and numerical work pertaining to photovoltaic cooling systems are given in References 5,16; some key contributions are noted here.

Cuce et al<sup>19</sup> reported on experiments conducted indoors using polycrystalline PV cells, demonstrating that both exergy and conversion efficiency were elevated respectively by 20% and 13%. Experiments by Chen et al<sup>21</sup> on naturally ventilated polycrystalline PV cells determined that heat transfer area and wind velocity were the main contributors affecting the performance of PV cells. Several studies<sup>22-26</sup> have employed active cooling via evaporation of water sprayed on the sun-facing surface of PV panels. This approach achieves up to a  $26^{\circ}\text{C}$  reduction in panel temperature.

Tonui and Tripanagnostopoulos<sup>27</sup> proposed modifications to the channel of a PV/T air system to increase thermal output and PV cooling. Conversion efficiency incremented by up to 6% using their fin system. Teo et al<sup>28</sup> developed a hybrid PV/T solar system to investigate active cooling of PV modules. An array of air ducts was affixed to the rear of the panels to establish forced convection. This system produced a temperature decrease from  $68^{\circ}\text{C}$  to  $38^{\circ}\text{C}$  and an efficiency boost from 8.6% to 12.5%. Tarabsheh et al<sup>29</sup> examined the performance of PV modules whose PV cells operate under different temperatures and proposed cooling pipe layouts underneath the PV module to improve the conversion efficiency of the module. Their results showed that the active cooling increased the efficiency by approximately 17%.

Bahaidarah et al<sup>30</sup> employed simulation and experiments to investigate a hybrid water-cooled PV system. The results showed a reduction in operating temperature of 20% and an increase of 9% in the electrical efficiency

with active cooling. Under a solar irradiance of  $900\text{ W/m}^2$ , cooling increased power output by 11.1%. More recently, Idoko et al<sup>31</sup> employed a combination of water-spray and a rear-mounted heat sink, achieving power output enhancement of approximately 21% and an efficiency gain exceeding 3%.

Jamali et al<sup>32</sup> suggested a new design of hybrid solar chimney system integrated with semi-transparent photovoltaic panels (STPV). The PV panels were installed at the roof of the collector to utilize the air flowing underneath in cooling the panels. The decrease in temperature in the proposed system reached  $15^{\circ}\text{C}$ , and the obtained power enhancement reached 29%.

Another aero-based cooling technique was proposed by Sajjad et al<sup>33</sup> through using the air leaving an air conditioner. The system resulted in an enhancement in the electrical power up to 7.2 W and 6% increase in the performance ratio.

El Mays et al<sup>34</sup> carried out an experimental investigation on a PV module equipped with a parallel-finned plate attached to the rear side under natural convection conditions. The results showed that the decrease in the frontside temperature was  $61^{\circ}\text{C}$  leading to an increase in the conversion efficiency and electrical power output of 1.75% and 1.8 W, respectively.

Hernandez-Perez et al<sup>35</sup> examined the effect of different fins orientation on the module surface temperature and conversion efficiency under natural convection conditions. CFD simulation was used at first to obtain the best heat sink with the best performance, followed by an experimental investigation. It was found that the maximum reduction in temperature was around  $10^{\circ}\text{C}$  and the improvement in conversion efficiency was approximately 4%. Dida et al<sup>36</sup> conducted an experimental investigation on a passive cooling technique based on the effect of water vapor to enhance the performance of a PV module; it was reported that the module temperature was reduced by  $20^{\circ}\text{C}$  (26%), resulting in an increase in the electrical efficiency by 14.75%.

The previous studies of various cooling methods on PV panels reveal that performance enhancement studies using an optimized plate-fins heat sink for a hot climate condition are scarce.

The present study aims to investigate passive cooling effects numerically and experimentally on the performance of a PV module for hot climate conditions such as that of Kuwait with numerical verification. An optimized heat sink for sustainable natural convection is attached to the back of the panel to maximise the extraction of unwanted thermal energy, lowering the operating temperature and resulting in higher efficiency and power output. To the best of our knowledge, this study has not been considered before in the literature.

The paper is organized as follows: The methodology is presented in Section 2, followed by descriptions of the experimental setup in Section 2.5 and numerical procedure in Section 2.6. Results and discussion follow in Section 3, with conclusions drawn in Section 4.

## 2 | METHODOLOGY

### 2.1 | Voltage-current characteristic equations

The characteristic curves of a photovoltaic cell vary with the solar insolation and cell temperature. The  $I$ - $V$  characteristic equations are given as<sup>37</sup>

$$I = I_L - I_0(\exp(q(V + IR_s)/n\sigma T_{PV}) - 1) - \frac{V_{PV} + I_{PV}R_s}{R_{sh}}, \quad (1)$$

$$P_{PV} = V_{PV}I_{PV}. \quad (2)$$

Here  $I_L$  is the light-generated current,  $I_0$  is the diode saturation current,  $q$  is the electron charge,  $\sigma$  is the Boltzmann constant,  $n$  is the diode factor, while  $T_{PV}$ ,  $I_{PV}$ ,  $R_s$ ,  $R_{sh}$ ,  $V_{PV}$  and  $P_{PV}$  respectively represent the module temperature, current, series resistance, parallel resistance, output voltage, and power output.

### 2.2 | Heat sink optimization

A heat sink is a thermally conductive heat exchanger that is attached to a device to enhance the dissipation of unwanted heat to the surroundings found in myriad applications including refrigeration, heat engines and electronic devices.<sup>38</sup> The performance of a heat sink is enhanced by increasing the thermal conductivity or surface area of the fins, or the heat transfer coefficient between the fins and their surrounding fluid. Rectangular, triangular and parabolic fin profiles are common. Rectangular plate fins are the simplest solution (both in terms of cost and reliability<sup>39</sup>), and are the profile chosen for the present study. Figure 1 illustrates a rectangular plate fin heat sink.

Typically, it is desired to maximize the heat transfer rate from the fin array and to minimize the mass, volume and cost. Therefore, aluminium is chosen for the heat sink here as it offers a good compromise between these criteria.

References 39, 40 provide guidance for optimal spacing between fins for a heat sink having fin thickness much smaller than fin spacing over a plate area  $L \times W$ ,

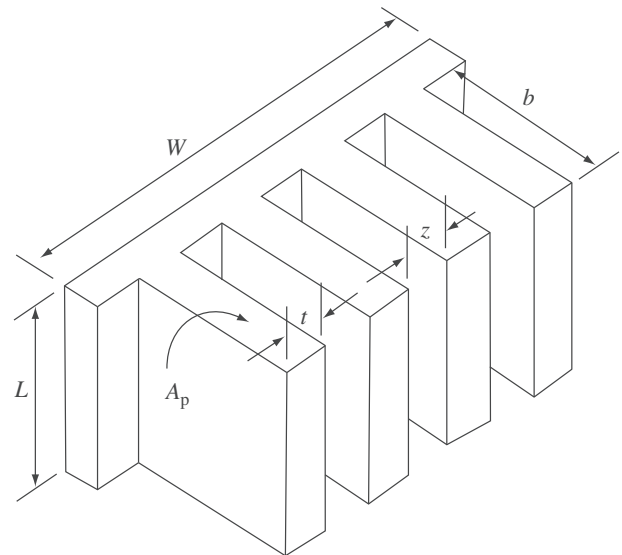


FIGURE 1 Schematic diagram of the plate-fin heat sink geometry with the dimensions: spacing  $z$ , thickness  $t$ , profile length  $b$ , profile area  $A_p$ , base plate length  $L$ , base plate width  $W$ <sup>38</sup>

$$z_{opt} = 2.714LRa_L^{-0.25}, \quad (3)$$

where the Rayleigh number for flow over a flat plate of length  $L$  is

$$Ra_L = \frac{g\beta(T_{base} - T_{\infty})L^3}{\nu\alpha}, \quad (4)$$

$\beta$  is the volumetric expansion coefficient,  $\alpha$  is the thermal diffusivity,  $\nu$  is the kinematic viscosity and  $g$  is acceleration due to gravity.  $T_{base}$  and  $T_{\infty}$  respectively denote the base plate and ambient air temperatures. Reference 40 also gives the optimum profile length as a function of optimum fin thickness  $t$ , as

$$b = \frac{1.4192 \left( \frac{K_f t}{2h_z} \right)^{1/2}}{\left[ 1 - 1.125 \left( \frac{K_f t}{2h_z} \right)^{1/2} \frac{h_z}{K_f} \right]}, \quad (5)$$

where  $K_f$  is the fin thermal conductivity and  $h_z$  is the heat transfer coefficient for a vertical parallel flow between two fins. In turn, this may be expressed as

$$h_z = \frac{K_a}{z_{opt}} \left( \frac{576}{El^2} + \frac{2.873}{El} \right)^{-1/2}, \quad (6)$$

where Elenbass number  $El = Ra_z z_{opt}/L$  and Rayleigh number based on the fin spacing is  $Ra_z = g\beta(T_{base} - T_{\infty})z_{opt}^3/\nu\alpha$ . The number of fins is also a function of fin thickness,

$$n_f = \frac{W}{z_{\text{opt}} + t}, \quad (7)$$

and the total mass of the material as a function of  $t$  is  $m_t = n_f \rho_f V_f$ , where  $V_f = Lbt$  is the volume of a single fin.

The single-fin efficiency, effectiveness and heat transfer are given, respectively, as

$$\eta_f = \frac{\tanh\left(b\sqrt{\frac{h_z(L+t)}{K_f L t}}\right)}{b\sqrt{\frac{h_z(L+t)}{K_f L t}}}, \quad (8)$$

$$Q_f = \eta_f h_z 2(L+t)b(T_{\text{base}} - T_{\infty}), \quad (9)$$

$$\varepsilon_f = \frac{Q_f}{h_z L t (T_{\text{base}} - T_{\infty})}. \quad (10)$$

The final equations for the overall efficiency  $\eta_o$ , total heat transfer  $Q_T$  rate and overall thermal resistance  $R_{th}$  are given in Reference 40 as

$$\eta_o = 1 - n_f \frac{A_f}{A_t} (1 - n_f), \quad (11)$$

with

$$A_f = 2(L+t)b, \quad (12)$$

$$A_t = \eta_f [2(L+t)b + Lz_{\text{opt}}], \quad (13)$$

where  $A_f$  and  $A_t$  are, respectively, the single-fin surface area and the total fin surface area,

$$Q_T = \eta_o h_z A_t (T_{\text{base}} - T_{\infty}), \quad (14)$$

$$R_{th} = \frac{1}{\eta_o h_z A_t}. \quad (15)$$

## 2.3 | PV cell efficiency

The efficiency of a PV cell is the ratio of its power output  $P_{PV}$  to the solar power striking the panel (the product of the irradiance  $G$  and area of the panel  $A_{pv}$ ),<sup>31</sup>

$$\eta_{PV} = \frac{P_{PV}}{GA_{pv}}. \quad (16)$$

The electrical power and efficiency depend on the ambient and PV cell working temperatures. This is due to

the dependence of the module voltage and current on temperature. The maximum power of the PV module can be expressed as<sup>41,42</sup>

$$P_{\text{max}} = V_m I_m = V_{ov} I_{sc} F_F, \quad (17)$$

where  $P_{\text{max}}$ ,  $V_m$  and  $I_m$  are the module maximum power, maximum voltage and maximum current, respectively,  $V_{ov}$  is the open circuit voltage,  $I_{sc}$  is the short circuit current, and  $F_F$  is the fill factor.

## 2.4 | Temperature dependence of PV cell efficiency

For the most common PV technology, crystalline silicon (c-Si), the temperature dependence of PV cell efficiency can be expressed as per<sup>43</sup> as

$$\eta_{PV} = \eta_R [1 - \beta_R (T_C - T_R) - \gamma \log_{10}(G)], \quad (18)$$

where  $\eta_R$  is the electrical efficiency of the PV module at reference temperature  $T_R$  (25°C), and  $\beta_R$  is a material-dependent temperature coefficient, typically in the range  $0.004 \lesssim \beta_R \lesssim 0.005/^\circ\text{C}$ .<sup>14,44</sup>  $T_C$  is the cell operating temperature,  $\gamma$  is a radiation intensity coefficient, and  $G$  is the irradiation incident on the PV module. By adding and subtracting the ambient temperature  $T_a$  to and from the temperature terms and setting  $\gamma = 0$ , Equation (18) reduces to<sup>14</sup>

$$\eta_{PV} = \eta_R \left[ 1 - \frac{G}{G_{NT}} (T_C - T_R) \beta_R (T_{C,NT} - T_{R,NT}) \right], \quad (19)$$

where  $G_{NT}$ ,  $T_{C,NT}$ , and  $T_{R,NT}$  are the solar irradiation, cell temperature and reference temperature at nominal operating temperature, respectively.

## 2.5 | Experimental setup

Two identical PV modules are employed in the experiments. The module specifications are provided in Table 1. The modules are each mounted as depicted in Figure 2. One module is coupled with an aluminium heat sink. Thermal grease is applied to the base of the heat sink, eliminating air gaps and preserving the integrity of thermal conductivity between the panel and heat sink. The heat sink was manufactured in the mechanical workshop of Australian College of Kuwait-ACK; its dimensions are given in Table 2.

The experiments were conducted during April 2019 in ACK, Mishref, within latitude 29.2761°N and

longitude 48.0654°E. The panels were oriented due south, tilted at 30° to the horizontal, and data was acquired from 6.00 AM to 5.00 PM on three separate days. The temperatures at the rear and front surfaces of the PV modules were recorded at 15-minute intervals using sensors and an Arduino microprocessor. Results were recorded from both panels simultaneously. The instrument devices used include Omega Type K thermocouples (accuracy ±0.8°C or 0.2%), voltage sensor, Allegro ACS721 current sensor (measuring between ±30 A), solar power meter (TES-132, having a 2000 W/m<sup>2</sup> range and 10 W/m<sup>2</sup> accuracy), rheostat, and Arduino Mega R3 (High Quality Clone) with multi pins.

The solar radiation was measured using a pyranometer located at the top of the PV modules. The temperatures on the rear and front surface of the PV modules were obtained using a six-channel data logger. The temperature probes were attached to the panels using a transparent tape to aid the accuracy of temperature measurements. Currents and voltages were obtained using current and voltage sensors and the Arduino microprocessor while variable resistors were used to reach the peak load of the PV panels. The Peak Power Point, 26.5 W, was found with a 2.1 Ω load which was used throughout the tests to evaluate the power outputs. Figure 3 shows the characteristic curves at 870 W/m<sup>2</sup>.

## 2.6 | Numerical procedure

Numerical thermal simulations were performed using the ANSYS 19.2 steady-state thermal solver. The steady-state thermal was conducted using a combination of LINK 33 and SURF 145 (film coefficient) mesh elements to simulate the conduction between the panel and the heat sink and the convection between the model and the ambient air. A simplified three-dimensional model of the PV panel and heat sink was meshed using ANSYS

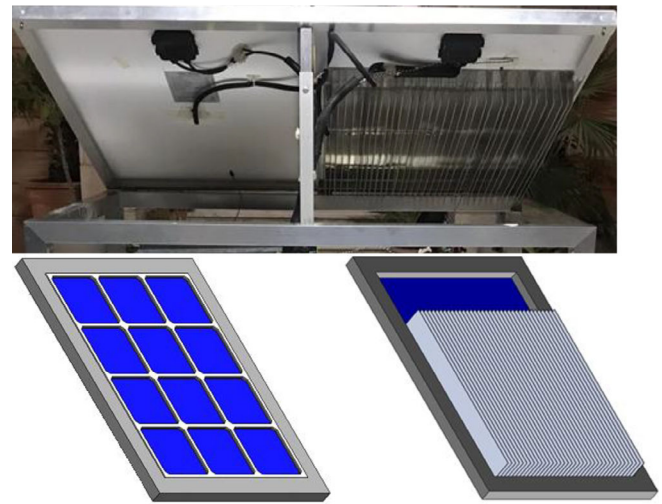


FIGURE 2 Photographs (top) and CAD models (bottom) of the experimental setup, showing the PV modules without (left) and with (right) the heat sink

workbench Design Modeler based on the dimensions given in Table 2.

The governing equation that describes the physical model and the boundary conditions may be written as

$$\rho c \left( u \frac{\partial T}{\partial x} + v \frac{\partial T}{\partial y} + w \frac{\partial T}{\partial z} \right) = \dot{Q} + K \left( \frac{\partial^2 T}{\partial x^2} + \frac{\partial^2 T}{\partial y^2} + \frac{\partial^2 T}{\partial z^2} \right), \tag{20}$$

where  $\dot{Q}$  is the rate of heat generation W/m<sup>3</sup>, which is obtained as

$$\dot{Q} = A_{PV} G \alpha \tau (1 - \eta_{PV}), \tag{21}$$

where  $\alpha$  and  $\tau$  are the absorptivity and transmissivity of the PV cell which are assumed to be 0.87 and 0.77, respectively.<sup>45</sup> A conversion efficiency  $\eta_{PV} = 15\%$  is assumed for the PV cell and the reference efficiency

TABLE 1 PV module technical data

Model number	FL-M-50 W
Maximum power, $P_{mp}$	50 W
Maximum power voltage, $V_{mp}$	18.0 V
Maximum power current, $I_{mp}$	2.77 A
Open circuit voltage, $V_{oc}$	21.60 V
Short circuit current, $I_{sc}$	2.94 A
Cell technology	Monocrystalline silicon
Module dimensions	710 × 540 × 30 mm
Module weight	3.60 kg

TABLE 2 Optimized heat-sink specifications

Fin thickness, $t$	0.8 mm
Profile length, $b$	75 mm
Fin spacing, $z$	13.6 mm
Number of fins, $n_f$	35.0
Mass of fins, $m_f$	3.98 kg
Length of heat sink, $L$	500 mm
Width of heat sink, $W$	495 mm

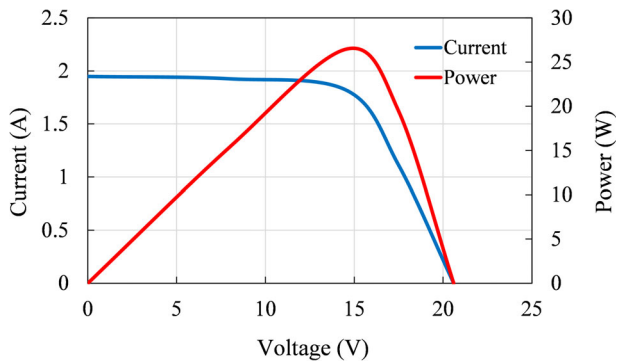


FIGURE 3 Characteristics of the PV module at  $S = 870 \text{ W/m}^2$ . Both electric current (blue line) and power (red line) are shown

$\eta_R = 12.5\%$  is assumed at a reference temperature  $T_R = 25^\circ\text{C}$ .<sup>46</sup>

The boundary conditions used in simulations are as follows: The module sidewalls were thermally insulated with a zero normal temperature gradient imposed on their surfaces, that is,

$$\frac{\partial T}{\partial n} = 0, \quad (22)$$

where  $n$  is the normal direction. The front and back surfaces are subjected to radiation and convection as

$$K \frac{\partial T}{\partial n} = h(T - T_\infty) + \varepsilon\sigma(T^4 - T_{\text{sky}}^4), \quad (23)$$

where  $T_\infty$  is the ambient temperature,  $T_{\text{sky}}$  is the sky temperature,  $\varepsilon$  is the surface emissivity and  $\sigma$  is the Stefan Boltzmann constant. A convective heat transfer  $h = 10 \text{ W m}^{-2} \text{ K}^{-1}$  and  $T_\infty = 32^\circ\text{C}$  were used at  $G = 1085 \text{ W m}^{-2}$  at 12.22 PM.

A grid resolution study was performed by varying the element size while keeping the number of elements unchanged. The maximum surface temperature was monitored for  $G = 1085 \text{ W m}^{-2}$  (corresponding to 12.22 pm in the experiments). It was found that results converged to within 0.1% with an average element size 3 mm and maximum element size 9 mm, which is used for the simulations reported in this study. The mesh was ultimately composed of 444030 tetrahedral elements and 520618 nodes, with mean element quality and skewness of 0.98 and  $1.3076 \times 10^{-10}$ , respectively. The distribution of the elements in the mesh employed in this study is shown in Figure 4.

To validate the numerical scheme being used, the numerical system was tested against the experimental measurements. The module average front surface temperature for the case with and without the heat sink were

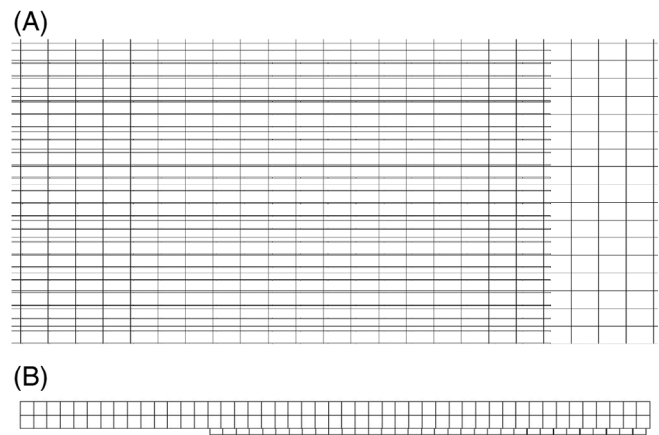


FIGURE 4 A plot showing the mesh of the PV module and heat sink. (A) Zoomed-in top view of a segment of the mesh. (B) Side view

compared against the experimental results recorded at 12.22 pm. A maximum error of less than 5% of the average temperatures between the numerical and experimental results was found. The numerical model was further validated using the results from<sup>34</sup> because their study includes both a standard PV panel and a PV panel integrated with a heat sink. The front temperature of the PV module for the case with and without heat sink were compared. Again, a very good agreement was found, and a maximum error of less than 5% was recorded between the results.

### 3 | RESULTS

Results will be presented in three parts. First, the dimensions of the passive cooling heat sink are determined with respect to the optimization parameters such as the total heat dissipation and fin effectiveness. Second, consideration will be given to the effect of passive cooling on the performance parameters of the PV modules such as the front and back temperatures, and maximum power. Finally, the increment in performance parameters will be presented.

To optimize the heat sink, the equations given in Section 2.2 are solved using Matlab. Figures 5 and 6 show the outcome of this optimization. The total heat dissipation rate is maximized for a given temperature difference (base to ambient) when the thermal resistance is minimized. This implies that the heat sink is capable of dissipating unwanted heat, lowering the operating temperature, which in turn increases the efficiency and power output.

Figure 5 shows the variation of total heat dissipation rate with the fin thickness at different fin profile lengths.

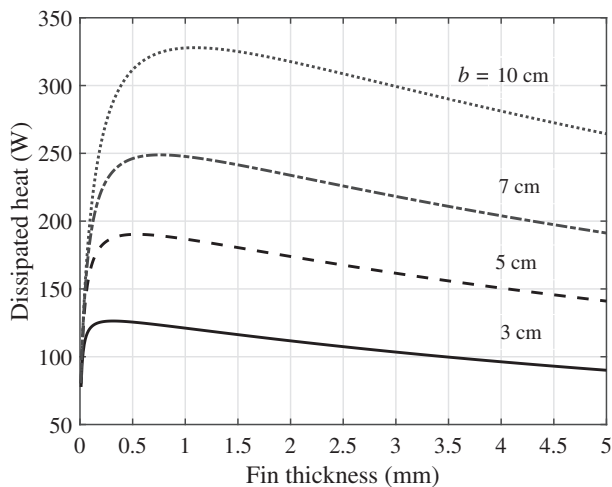


FIGURE 5 Optimization of the total heat dissipation of the heat sink at different fin profile lengths at  $z = 13.615$  cm and  $\Delta T = 20$  K

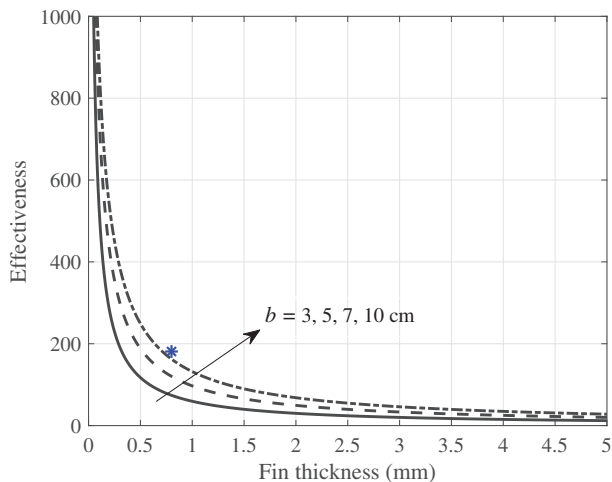


FIGURE 6 Optimization of the effectiveness of the heat sink at different fin profile lengths at  $z = 13.615$  cm. The characteristics of the current heat sink is represented by \*

It is apparent that heat dissipation across all fin thicknesses is strongly dependent on fin profile length. There is a diminishing return as  $b$  increases: notice for instance that dissipation peaks at 150 W at  $b = 5$  cm, only approximately 120 W is gained by doubling the fins to  $b = 10$  cm. Ultimately it was found that fins exceeding 20 cm did not produce further heat dissipation gains. The maximum heat dissipation occurs at small fin thickness, though the optimal thickness increases with fin length, presumably to allow higher thermal conduction through each fin to supply heat to its larger surface area.

The efficacy of a plate-fin heat sink may be characterized by the effectiveness,  $\epsilon_f$ , which is defined as the ratio of heat transfer for a plate with fins to a plate without,

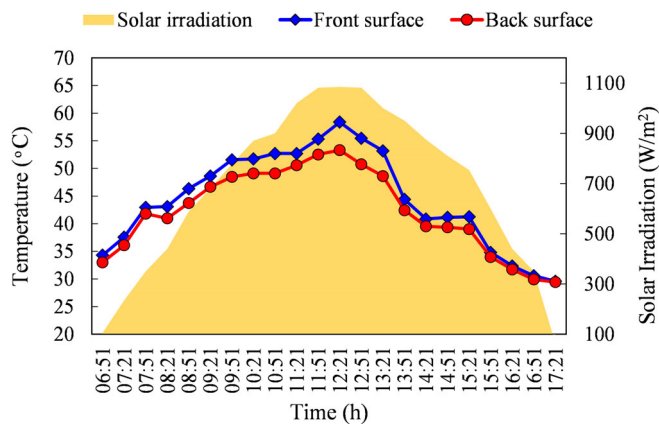
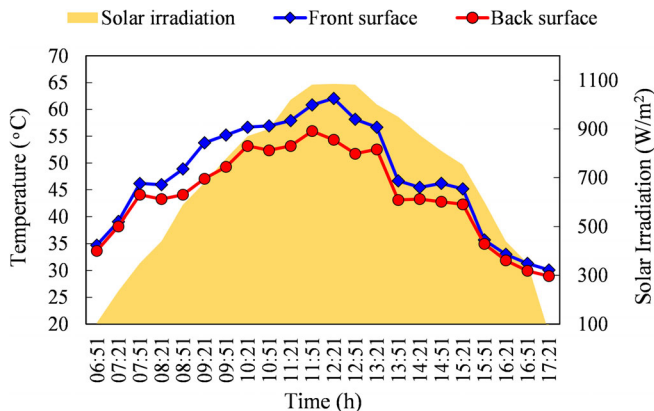


FIGURE 7 Front and rear temperatures of the PV panel with heat sink during the day. The bar chart shows the variation of solar irradiance during the day is overlaid in this graph

where  $\epsilon_f \gg 1$  is desired. The dependence of the heat sink effectiveness on the fin thickness at different profile lengths is shown in Figure 6. An effectiveness  $\epsilon_f \gg 1$  is observed at small fin thickness for all  $b$ . For the present heat sink, where  $b = 75$  mm and  $t = 0.8$  mm, the effectiveness is  $\epsilon_f \approx 180$ ; hence the current heat sink is expected to be highly effective at increasing the heat transfer rate and dissipating heat at the given temperature difference.

Now the effect of using a heat sink on the PV module temperatures (front and back) and maximum power output will be considered. The temperature variations for both PV panels is depicted along with solar irradiation data respectively in Figures 7 and 8 for the two setups. The maximum value of solar irradiation received is  $1085 \text{ W/m}^2$  at 12.21 PM, whereas the average throughout the day was  $685 \text{ W/m}^2$ . The sun-facing front surface correspondingly experiences higher temperatures than the rear surface.

At the start of the experiment, the temperature of both modules was almost identical. Subsequently, a progressive deviation between the module temperatures is observed. For the control case (no heat sink), a maximum surface temperature of approximately  $62^\circ\text{C}$  was recorded, while the rear surface measured  $56^\circ\text{C}$ . By contrast, the module affixed with the heat sink reaches front and rear maximum temperatures of  $58^\circ\text{C}$  and  $53^\circ\text{C}$ , respectively. Cooling the module with the heat sink has reduced the surface temperatures. In addition, addition of the heat sink also spreads out the heat dissipation over the rear of the panel, reflected by the greater uniformity in the temperature distribution seen in Figure 9, where contours of temperature distribution over the PV panel with and without the heat sink are displayed at the point of maximum solar irradiance. The PV panel without the heat



**FIGURE 8** Front and rear temperatures of the PV panel without heat sink during the day. The bar chart shows the variation of solar irradiance during the day is overlaid in this graph

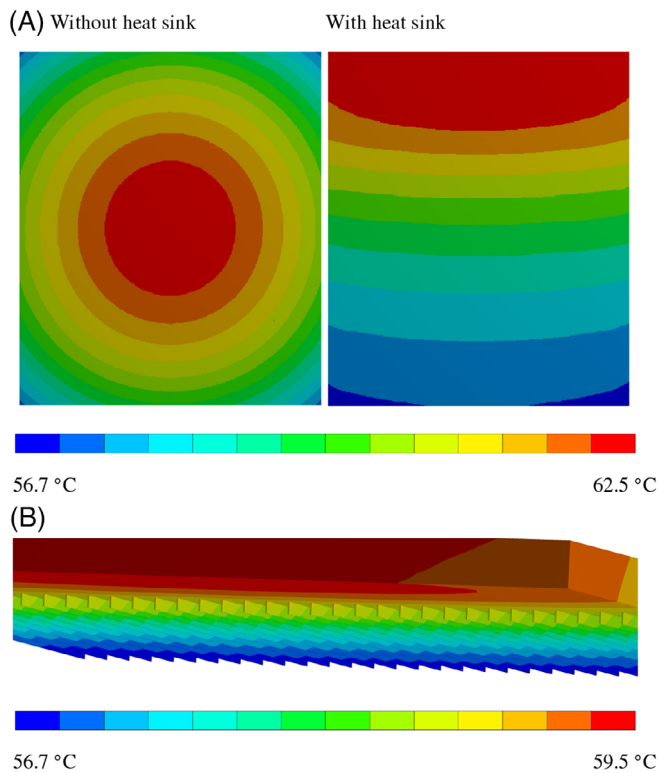


**FIGURE 9** (A) Contours of temperature for the PV panels (left) without and (right) with the heat sink. (B) Three-dimensional visualisation of the setup coloured by temperature. These cases model the maximum measured solar irradiance  $G = 1058 \text{ W/m}^2$  at 12.22 PM

sink is hottest at its centre, whereas the panel with the heat sink is relatively cooler across much of its surface, only being hot at the top region that extended beyond the coverage of the heat sink.

The temperature reduction resulted in an appreciable improvement in the efficiency and power output of the

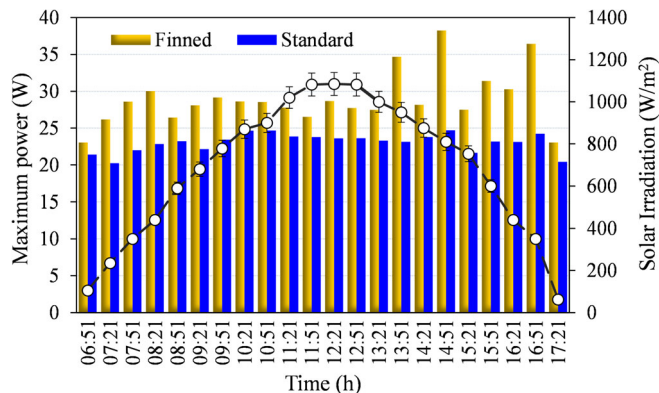


**FIGURE 10** Comparison of maximum power output of the module  $P_{\text{max}}$  during the day with and without heat sink. The dashed-line curve shows the variation of irradiance during the day

PV module, as seen in Figures 10 and 11. Figure 10 compares the maximum electrical power output of the module for the two cases during the test day. As discussed in Sections 2.3 and 2.4, the maximum power output of the module changes with the intensity of solar irradiance and the surface temperature of the cell. It is also affected by the number of cells in the module, the type of cells, and the total surface area of cells. The peak power of a module is rated by manufacturers under standard test conditions of  $1000 \text{ W/m}^2$  solar irradiance and  $25^\circ\text{C}$  cell temperature. Therefore, the maximum power output produced by the module is always less than that of the rated peak power under real conditions. The maximum value of the power output for the case without a heat sink was  $24.71 \text{ W}$  at 2:51 PM whereas the maximum power output with the heat sink was  $38.25 \text{ W}$ .

In order to characterize the effect on the maximum power output and maximum efficiency due to the addition of the heat sink, the percentage increment of the power output and efficiency are presented in Figure 11. A maximum increase in the solar to the electrical conversion efficiency of 35% and 55% in the power output were achieved with the use of a heat sink while the respective average increase in the power and efficiency were almost 26% and 20%.

The total increase in kilowatt-hours by the PV module with the heat sink over the time of the experiments was  $4.3 \text{ kWh/m}^2/\text{day}$ , and the annual system output was  $1565 \text{ kWh/m}^2/\text{yr}$ . Based on the current electricity cost in Kuwait, which is  $\$0.03/\text{kWh}$ , the total yearly saving was  $\$47/\text{m}^2/\text{yr}$ . With a 4 kW solar system, the annual saving can be  $\$1316$ . The parameters used to estimate the power of the solar system are as follow: average roof area =  $28 \text{ m}^2$  number of modules per PV system =  $28/0.35 = 80$  modules. With a module of a maximum power of 0.05 kW, the system power is  $80 \times 0.05 \text{ kW}$ .

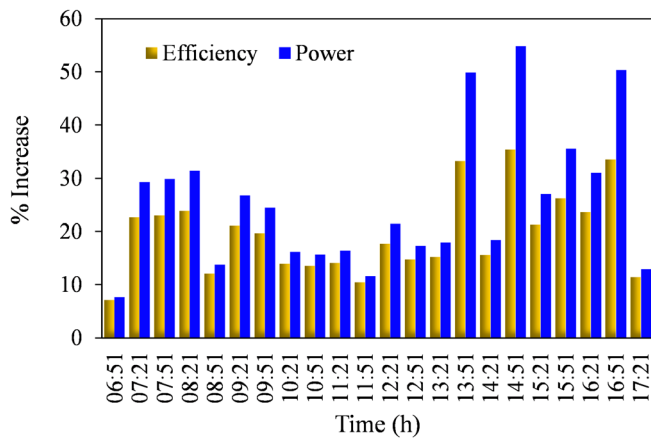


**FIGURE 11** Percentage increment of the maximum efficiency and maximum power output obtained by adding the heat sink to the of the PV module during the day

To demonstrate the commercial viability of the heat sink addition to PV panels, other regions worldwide with similar climates are also estimated. The annual saving in southern Australia, northern Africa, and the southern USA can be \$11088, \$1988, \$6850, respectively, based on a respective energy cost of \$0.253/kWh, \$0.045/kWh, and \$0.150/kWh. It is important to emphasize that savings are much more significant than the extra cost incurred on the PV-heat sink system to regulate the temperature. It is only cost 25% to 30% of the PV purchase cost when mass-produced.

## 4 | CONCLUSIONS

In this study, effects of passive cooling on the performance parameters of PV module are investigated experimentally and numerically using an optimized plate fins heat sink. The dimensions of the heat sink are optimized and determined with respect to parameters such as the total heat dissipation and fin effectiveness. The effect of incorporating a heat sink with the PV module is investigated experimentally. Efficiency and maximum power output with and without heat sink are determined and the results are compared. The PV surface temperature was observed to significantly alter the conversion efficiency and the maximum power output. It was found that cooling the module with the heat sink resulted in an average reduction of the front and back temperature by respectively 4% and 6.5 which in turn lead to a marked improvement in the efficiency and power output of the PV panel. A maximum increase in the solar to electrical conversion efficiency of 35% and approximately 55% in the power output were achieved with the use of a heat

sink. The tests of the effectiveness of the heat sink suggest that even greater performance improvement might be possible with longer fins than those considered in this study. The economic analysis for a 4 kW solar system shows that in Kuwait, the annual saving is less than other regions in the world that have a similar climatic condition. The suggested cooling system is expected to be more beneficial and attractive in regions like southern Australia and the southern USA.

## ACKNOWLEDGEMENTS

The authors acknowledge the financial support provided by Kuwait Foundation for the Advancement of Sciences (grant PN19-35EM-02). The authors also would like to acknowledge the support of Australian College of Kuwait through the Mechanical Engineering Department. Gregory J. Sheard is supported by the Australian Research Council through Discovery Grant DP180102647.

## ORCID

Wisam K. Hussam  <https://orcid.org/0000-0001-6121-4385>

## REFERENCES

1. Ramadhan M, Hussain A. Kuwait energy profile for electrical power generation. *Strateg Plan Energy Environ*. 2012;32:18-25.
2. Otaibi AA, Jandal SA. Solar photovoltaic power in the State of Kuwait. Paper presented at: 37th IEEE Photovoltaic Specialists Conference. 2011, 003091-003096.
3. Ghoneim A, Kadad I, Altouq M. Statistical analysis of solar UVB and global radiation in Kuwait. *Energy*. 2013;60:23-34.
4. Ouhsaine L, Mimet A, Ganaoui ME, Scipioni A, Kharbouch Y. Transient thermal analyse of mini heat sink PV cells cooling for hot climate. Paper presented at: International Renewable and Sustainable Energy Conference (IRSEC). 2014: 70-77.
5. Abhishek A, Amritanshu S, Panchal H, Sharma A. Thermal regulation of photovoltaic system for enhanced power production: a review. *J Energy Storage*. 2021;35:102236.
6. Radziemska E, Klugmann E. Thermally affected parameters of the current-voltage characteristics of silicon photocell. *Energy Convers Manag*. 2002;43:1889-1900.
7. Radziemska E. The effect of temperature on the power drop in crystalline silicon solar cells. *Renew Energy*. 2003;28:1-12.
8. Skoplaki E, Palyvos J. On the temperature dependence of photovoltaic module electrical performance: a review of efficiency/power correlations. *Sol Energy*. 2009;83:614-624.
9. El-Adawi M, Al-Nuaim I. The temperature functional dependence of VOC for a solar cell in relation to its efficiency new approach. *Desalination*. 2007;209:91-96.
10. Cuce E, Bali T. Variation of cell parameters of a p-Si PV cell with different solar irradiances and cell temperatures in humid climates. Paper presented at: Fourth International Exergy, Energy and Environment Symposium. 2009, 19-23.
11. Rajput U, Yang J. Comparison of heat sink and water type PV/T collector for polycrystalline photovoltaic panel cooling. *Renew Energy*. 2018;116:479-491.

12. Nižetić S, Papadopoulos A, Giama E. Comprehensive analysis and general economic-environmental evaluation of cooling techniques for photovoltaic panels, part I: passive cooling techniques. *Energy Convers Manag.* 2017;149:334-354.
13. Makrides G, Zinsser B, Norton M, Georghiou G. Performance of photovoltaics under actual operating conditions. *Third Generation Photovoltaics.* 2012, 201–232.
14. Kaldellis J, Kapsali M, Kavadias K. Temperature and wind speed impact on the efficiency of PV installations. Experience obtained from outdoor measurements in Greece. *Renew Energy.* 2014;66:612-624.
15. Mercaldo L, Addonizio M, Noce MD, Veneri P, Scognamiglio A, Privato C. Thin film silicon photovoltaics: architectural perspectives and technological issues. *Appl Energy.* 2009;86:1836-1844.
16. Kandeal A, Thakur A, Elkadeem M, et al. Photovoltaics performance improvement using different cooling methodologies: a state-of-art review. *J Clean Prod.* 2020;273:122772.
17. Makrides G, Zinsser B, Georghiou G, Schubert M, Werner JH. Temperature behaviour of different photovoltaic systems installed in Cyprus and Germany. *Sol Energy Mater Sol Cells.* 2009;93:1095-1099.
18. Virtuani A, Mullejans H, Dunlop E. Comparison of indoor and outdoor performance measurements of recent commercially available solar modules. *Prog Photovolt Res Appl.* 2011;19(1):11-20.
19. Cuce E, Bali T, Sekucoglu S. Effects of passive cooling on performance of silicon photovoltaic cells. *Int J Low-Carbon Technol.* 2011;6:299-308.
20. Kumar R, Priyadharshini N, Natarajan E. Experimental and numerical analysis of photovoltaic solar panel using thermoelectric cooling. *Indian J Sci Technol.* 2015;8:252-256.
21. Chen H, Chen X, Li S, Ding H. Comparative study on the performance improvement of photovoltaic panel with passive cooling under natural ventilation. *Int J Smart Grid Clean Energy.* 2014;4:374-379.
22. Odeh S, Behnia M. Improving photovoltaic module efficiency using water cooling. *Heat Transfer Eng.* 2009;30:499-505.
23. Kordzadeh A. The effects of nominal power of array and system head on the operation of photovoltaic water pumping set with array surface covered by a film of water. *Renew Energy.* 2010;35:1098-1102.
24. Dorobanțu L, Popescu M. Increasing the Efficiency of Photovoltaic Panels through Cooling Water Film. *UPB Sci. Bull., Series C.* 2013, 75.
25. Aldihani A, Aldossary A, Mahmoud S, Al-Dadah R. The effect of cooling on the performance of photovoltaic cells under dusty environmental conditions. *Energy Procedia.* 2014;61:2383-2386.
26. Irwan M, Leow W, Irwanto M, Amelia A, Gomesh N, Safwati I. Indoor test performance of pv panel through water cooling method. *Energy Procedia.* 2015;79:604-611.
27. Tonui J, Tripanagnostopoulos Y. Air-cooled PV/T solar collectors with lowcost performance improvements. *Sol Energy.* 2007; 81(4):498-511.
28. Teo H, Lee P, Hawlader M. An active cooling system for photovoltaic modules. *Appl Energy.* 2012;90:309-315.
29. Tarabsheh AA, Voutetakisb S, Papadopoulosb A, Seferlisb P, Etiera I, Saraereha O. Investigation of temperature effects in efficiency improvement of non-uniformly cooled photovoltaic cells. *Chem Eng Trans.* 2013;35:1387-1392.
30. Bahaidarah H, Subhan A, Gandhidasan P, Rehman S. Performance evaluation of a PV (photovoltaic) module by back surface water cooling for hot climatic conditions. *Energy.* 2013;59:445-453.
31. Idoko L, Anaya-Lara O, McDonald A. Enhancing PV modules efficiency and power output using multi-concept cooling technique. *Energy Rep.* 2018;4:357-369.
32. Jamali S, Yari M, Mahmoudi SMS. Enhanced power generation through cooling a semi-transparent PV power plant with a solar chimney. *Energy Convers Manag.* 2018;175:227-235.
33. Sajjad U, Amer M, Ali H, Dahiya A, Abbas N. Cost effective cooling of photovoltaic modules to improve efficiency. *Case Stud Therm Eng.* 2019;14:100420.
34. El Mays A, Ammar R, Hawa M, et al. Improving photovoltaic panel using finned plate of aluminum. *Energy Procedia.* 2017; 119:812-817.
35. Hernandez-Perez J, Carrillo J, Bassam A, Flota-Banuelos M, Patino-Lopez L. A new passive PV heatsink design to reduce efficiency losses: a computational and experimental evaluation. *Renew Energy.* 2020;147:1209-1220.
36. Dida M, Boughali S, Bechki D, Bouguettaia H. Experimental investigation of a passive cooling system for photovoltaic modules efficiency improvement in hot and arid regions. *Energy Convers Manag.* 2021;243:114328.
37. Walker G. Evaluating MPPT converter topologies using a MATLAB PV model. *J Electron Electr Eng.* 2001;21:49-56.
38. Bejan A, Tsatsaronis G, Moran M. *Thermal Design and Optimization.* New York, NY: John Wiley & Sons; 1996.
39. Bar-Cohen A, Iyengar M. Design and optimization of air-cooled heat sinks for sustainable development. *IEEE Trans Compon Packag Technol.* 2002;25(4):584-591.
40. Bar-Cohen A, Iyengar M, Kraus A. Design of optimum plate-fin natural convective heat sinks. *J Electron Packag.* 2003; 125(2):208-216.
41. Sethi V, Sumathy K, Yuvarajan S, Pal D. Mathematical model for computing maximum power output of a PV solar module and experimental validation. *J Fundam Renew Energy Appl.* 2012;2:1-5.
42. Dubey S, Sarvaiya J, Seshadri B. Temperature dependent photovoltaic (PV) efficiency and its effect on PV production in the world—a review. *Energy Procedia.* 2013;33:311-321.
43. Evans D. Simplified method for predicting photovoltaic array output. *Sol Energy.* 1981;27:555-560.
44. Hove T. A method for predicting long-term average performance of photovoltaic systems. *Renew Energy.* 2000;21:207-229.
45. Duffie J, Beckman W, Blair N. *Solar Engineering of Thermal Processes, Photovoltaics and Wind.* Hoboken, NJ: John Wiley & Sons; 2020.
46. Hegazy A. Comparative study of the performances of four photovoltaic/thermal solar air collectors. *Energy Convers Manag.* 2000;41:861-881.

**How to cite this article:** Hussam WK, Khlefat AM, Sheard GJ. Energy saving and performance analysis of air-cooled photovoltaic panels. *Int J Energy Res.* 2022;46(4):4825-4834. doi:10.1002/er.7475